



1 **Shift in seasonal snowpack melt-out date due to light-absorbing particles at a high-altitude site**
2 **in Central Himalaya**

3 Johan Ström¹, Jonas Svensson^{2,3}, Henri Honkanen⁴, Eija Asmi², Nathaniel B. Dkhar⁵, Shresth Tayal^{5,6},
4 Ved P. Sharma^{5,6}, Rakesh Hooda², Outi Meinander², Matti Leppäranta⁴, Hans-Werner Jacobi³, Heikki
5 Lihavainen^{7,2}, Antti Hyvärinen²

6

7 1 Department of Environmental Science, Stockholm University, Stockholm, Sweden

8 2 Atmospheric Composition Research, Finnish Meteorological Institute, Helsinki, Finland

9 3 Université Grenoble-Alpes, CNRS, IRD, INP-G, IGE, Grenoble, 38000, France

10 4 Institute for Atmospheric and Earth System Research, Faculty of Science, University of Helsinki, Helsinki,
11 Finland

12 5 The Energy and Resource Institute, (TERI) New Delhi, India

13 6 TERI School of Advanced Studies (TERI SAS), New Delhi, India

14 7 Svalbard Integrated Arctic Earth Observing System, Longyearbyen, Norway

15

16 Correspondence to: jonas.svensson@fmi.fi

17

18 *Abstract*

19 Snow darkening by deposited light-absorbing particles (LAP) has the potential to accelerate snowmelt and shift
20 the snow melt-out date. Here we investigate the sensitivity of the seasonal snow cover duration to changes in
21 LAP at a high altitude valley site in the Central Himalayas, India. First, the variation of the albedo of the seasonal
22 snow was emulated using two seasons of automatic weather station (AWS) data and applying a constant, but
23 realistic deposition of LAP to the snow. Then, the number of days with snowmelt were evaluated based on the
24 estimated net energy budget of the seasonal snow cover and the derived surface temperature. The impact on the
25 energy budget by LAP combined with the melt-day analysis resulted in very simple relations to determine the
26 contribution of LAP to the number of days with snowmelt of the seasonal snow in Himalaya. Above a
27 concentration of 1 ng g^{-1} (Elemental Carbon equivalent, EC_{eq} , which in this study includes EC and the absorption
28 equivalent EC contribution by other light absorbing particles, such as mineral dust) in new snow, the number of
29 days with snowmelt can be estimated by: $days = 0.0109(\log(EC_{eq}) + 1)PP \pm 0.0033(\log(EC_{eq}) + 1)PP$,
30 where PP is the seasonal precipitation in mm snow water equivalent. A change in EC_{eq} by a factor of two
31 corresponds to about $\frac{1}{3}$ of a day per 100 mm precipitation. Although the change in the number of days with melt
32 caused by the changes in EC_{eq} is small, the estimated total change in the snow melt-out date by LAP can be
33 significant. For our realistic base case scenario for the Sunderdhunga Valley, Central Himalayas, India, of
34 $EC_{eq}=100 \text{ ng g}^{-1}$ and $PP=400 \text{ mm}$, this yields in an advancement of the melt-out date of about 13 days.



35 1. Introduction

36 Seasonal snow cover in the Himalaya is an integral component of the regional hydrological cycle, with the
37 timing of the melting phase being crucial for the supply of fresh water with growing importance at increasing
38 altitudes (e.g. Armstrong et al., 2018; Mimeau et al., 2019). Replacing a bright snow surface for a darker soil
39 surface drastically changes the local climate. The albedo of snow has a key role in the energy balance of the
40 snow pack, and may be the main controller of snow melt (Cuffey & Paterson, 2010). Strongly dependent on the
41 microphysical properties of snow (e.g. snow liquid water content, grain size, and shape; Aoki et al., 2003), the
42 albedo is also affected by the presence of light-absorbing particles (LAP) (Warren & Wiscombe, 1980).
43 Originating mostly from anthropogenic emissions, LAP can be transported from distant source regions before
44 being mixed with snow, making this factor particularly interesting with regards to a potential human influence
45 on the regional climate and hydrological cycle. The two main components of LAP in the Himalaya are mineral
46 dust (MD) and light-absorbing carbonaceous particles. Whereas MD can be regarded as having mainly natural
47 sources, black or brown carbon (BC, BrC) are mainly attributed to human activities associated with the
48 combustion of biomass and fossil fuels, although natural wild-fires can also be a very significant source of BC
49 and BrC.

50 A common technique to analyze carbonaceous particles in snow is to use a thermo-optical method that yields
51 the mixing ratio of elemental carbon (EC) to the melted snow volume/mass, or snow water equivalent (SWE)
52 commonly expressed as, $\mu\text{g L}^{-1}$, ng g^{-1} , or ppb_w (e.g. Forsström et al., 2009; Ming et al., 2008). Because EC is
53 the main light absorbing component of BC, these acronyms are sometimes used interchangeably in the literature,
54 although BC most commonly refers to optically detected LAP (see e.g. Petzold et al., 2013). In addition, the
55 refractory component of BC (rBC) in snow can be determined (e.g. Schwarz et al., 2012). Here we work with
56 EC or the equivalent EC (EC_{eq}). The latter is the sum of EC and the absorption equivalent EC contribution by
57 MD or other light absorbing components (as measured in Svensson et al. 2018; 2021).

58 Snow darkening by BC in the Himalayan cryosphere has been shown to significantly vary regionally (e.g.
59 Gertler et al., 2016). The other main LAP constituent, MD, was recently identified as the dominating light
60 absorber in the snow above 4000 m altitude for High Mountain Asia (Sarangi et al. 2020). In contrast, Schmale
61 et al. (2017) reported BC as the main particle absorber in measurements of glacier snow samples from
62 Kyrgyzstan, Central Asia. The authors also presented a model to estimate the fraction of snowmelt attributable
63 to LAP. The model took into account the absorptivity of the snow and the amount of incoming shortwave
64 radiation, as well as the number of days with a temperature above 0 °C, to estimate a summer snowmelt rate
65 increase of up 6.3% due to LAP. This model has been applied over the Tibetan plateau with different SWE and
66 shortwave radiation scenarios (220, 270, and 310 W m^{-2}) for BC and MD (Zhang et al., 2018). That study present
67 a range of 1.3 - 1.8 days of reduction in average snow cover duration (SCD) for a SWE of 40 mm due to BC
68 and MD, whereas for a 100 mm SWE the SCD reduction was 3.1 - 4.4 days. It is further concluded that the
69 reductions in SCD is mainly because of BC, and not MD, for that area. Similarly the model was used in Northern
70 Xinjiang, China, with different SWE and shortwave radiation scenarios for BC and MD, shortening the SCD in



71 the range of 1.4 ± 0.6 to 6.1 ± 3.4 days (Zhong et al., 2019). As a comparison, a different approach to estimate
72 the reduced snow cover was presented by Ménéguez et al. (2014). Utilizing a climate-chemistry global model to
73 approximate the effect from BC deposition on the Himalayan snow cover, they found an annual reduction in
74 SCD by 1 to 8 days. The authors conclude that the low precipitation rates of snow over the Tibetan Plateau
75 contribute to the low number, while anthropogenic BC is expected to have a larger effect in the mountain ranges
76 (Himalaya, Karakoram, Hindu-Kush).

77 Common for the studies summarized above is that they are based on an extensive dataset and/or complex
78 numerical models, and that the results are not generalized. Here we study the influence by LAP on the seasonal
79 snow cover duration with a different approach, attempting to reduce the information needed and at the same
80 time generalizing the results. We use two seasons of automatic weather station (AWS) data from the
81 Sunderdhunga Valley at about 4700 m altitude in central Himalaya, as well as observations on LAP in the glacier
82 snow from the same valley (Svensson et al., 2021), to investigate the sensitivity of seasonal snow cover duration
83 to changes in EC_{eq} . Through analysis of these two seasons and a series of assumptions and simplifications, the
84 complex system of LAP and albedo reduction is condensed down into a dependence of only a few variables.
85 With these simplified relations we attempt to answer the question: what is the contribution to the number of
86 days with snowmelt from a given change of LAP in the seasonal snow for the study region?

87 The analysis is conducted in two main sections. Section 3 presents how a parametric description of the daily
88 variation in albedo is formulated (with taking into account LAP and ground albedo) and how that albedo
89 compares to the observed albedo. Section 4 presents how the data is analyzed with respect to the number of days
90 with melt associated with each season. The results are combined into simple relations to estimate the influence
91 on the contribution of LAP to the number of days with snowmelt, based on the LAP content in the snowpack
92 and the seasonal precipitation.

93 2. Observations

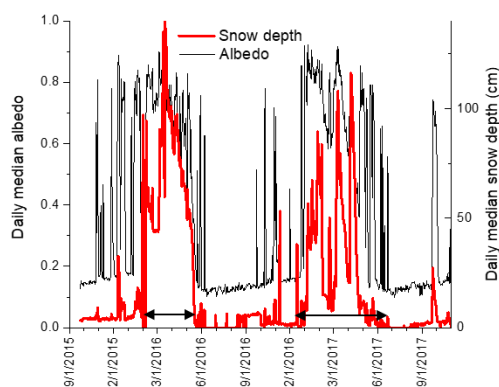
94 2.1 Automatic weather station

95 The AWS observations are from the immediate vicinity (~ 100 m) of the glacier ablation zone of Durga Kot
96 glacier in the Sunderdhunga valley, northern India, further described in Svensson et al. (2021). Two seasonal
97 snow cover periods are utilized here (indicated by arrows in Figure 1), lasting between 6 February 2016 and 22
98 May 2016 (season 1), and between 24 December 2016 and 1 June 2017 (season 2). The AWS is equipped with
99 instrumentation for air temperature (T_a), relative humidity (RH) (HC2S3-L Temperature and relative humidity
100 probe manufactured by Rotronic, with 41303-5A Radiation shield), broadband shortwave radiation upward and
101 downward (SW_u , SW_d) and longwave radiation upward and downward (LW_u , LW_d) (CNR4 Four-component
102 net radiometer manufactured by Kipp & Zonen), snow depth (SD) (Campbell Scientific SR50A-L Ultrasonic
103 Distance Sensor), wind speed (U), and wind direction (not used in this paper) (05103-L Wind monitor
104 manufactured by R. M. Young). Data was logged every 10 minutes and screened for inconsistencies, which may
105 arise, for example, from snow covering the sensors. Subsequently, the data was averaged over each day, expect



106 for albedo and SD which are based on daily median values. The time series of albedo and SD are presented in
107 Figure 1.

108 Based on LW_u and assuming unit emissivity of snow, the Stephan-Boltzmann's Law (supplement equation 1)
109 is used to calculate a representative surface temperature (T_s). Using a lower emissivity would result in higher
110 T_s , but will not affect the interpretation of the data. Precipitation was not explicitly measured at this location,
111 but is estimated similar to the method described in Svensson et al. (2021), yielding an estimate of the amount
112 of precipitation in mm SWE (PP). The positive changes in snow depth (SD^+) are integrated over the periods in
113 question and the density of the new snow is assumed to be 100 kg m^{-3} (Helfricht, et al., 2018). The estimated
114 total PP for season 1 and season 2 are 290 and 460 mm, respectively. The measured AWS variables recorded
115 during the two seasons are further presented in supplement Figure S1.



116

117 Figure 1. Daily median albedo and snow depth from 22 September 2015 to 31 October 2017. The period
118 considered for the two seasonal snow covers are indicated with the black double arrow lines.

119 2.2 Light-absorbing particles

120 The basis for LAP in the snow for this study originates from observations reported in Svensson et al. (2021).
121 They showed that LAP in young snow (interpreted as snow from the current winter season), sampled at Durga
122 Kot and the neighboring Bhanolti glacier at a distance about 1-2 km due southwest from the AWS at about 5000
123 m altitude, can be described by a characteristic constant deposition of EC of about $50 \mu\text{g m}^{-2} \text{ PP}^{-1}$. In other
124 words, each mm of precipitation contains an EC concentration of 50 ng g^{-1} . For both winter seasons the dry
125 deposition of EC likely contributed small amounts to the overall deposition of EC as proposed in Svensson et
126 al. (2021). Using a dry deposition velocity of BC of 0.3 mm/s (Emerson et al., 2018) and an atmospheric
127 concentration of $0.3 \mu\text{g m}^{-3}$, reported at the Nepal Pyramid station during the pre-monsoon (Bonasoni et al.,
128 2010), the dry deposition can be estimated to contribute to EC by $845 \mu\text{g m}^{-2}$ and $1236 \mu\text{g m}^{-2}$ for season 1 and
129 2, respectively. Comparison to the EC wet deposition estimates for seasons 1 and 2: $14500 \mu\text{g m}^{-2}$ and 23000
130 $\mu\text{g m}^{-2}$ (obtained by multiplying $50 \mu\text{g m}^{-2}$ with the PP of each season), suggests that EC dry deposition is on
131 the order of 5-6% of the total EC deposition. The two analyzed seasons here represent the main precipitation



132 periods of the year for this site, further supporting the argument that dry deposition is not significant for our
133 investigations.

134

135 3. Albedo parameterization

136 3.1 Effective grain size, pristine albedo and specific surface area of snow

137 For snow, the effective grain size (r_e) can be estimated by the ratio between volume and area according to

$$138 r_e = \frac{3}{\rho_i SSA} \quad (1)$$

139 Where ρ_i is the density of ice (910 kg m^{-3}), and SSA is the specific surface area of snow ($\text{m}^2 \text{ kg}^{-1}$). The
140 formulation proposed by Gardner and Sharp (2010) relates the albedo of pristine snow (a_p) to variations in SSA
141 as

$$142 a_p = 1.48 - SSA^{-0.07} \quad (2)$$

143 where a_p is the albedo of pristine snow (i.e. without LAP) and SSA is given in ($\text{cm}^2 \text{ g}^{-1}$). Liquid water in snow
144 influence the albedo indirectly by enhancement of r_e and filling voids between the snow crystals (Colbeck,
145 1979). Changes in r_e , SSA and a_p are often parameterized using variations of summed daily maximum
146 temperatures since the last snow fall to capture the metamorphism of the snow over time (e.g. Winter, 1993;
147 Brock et al., 2000). We are interested in a relation that directly connects our AWS observations to the grain size
148 of pristine snow. Therefore, we explore to diagnose SSA for pristine snow as function of T_a or T_s based on our
149 own data set. This is done by grouping the data in one degree temperature bins using all available data (from 22
150 September 2015 to 31 October 2017). For each temperature bin, the maximum albedo was identified and the
151 corresponding SSA was calculated with eq. 2. The logarithm of the SSA is presented in supplement Figures S2a
152 and S2b as a function of temperature. The maximum albedo for each temperature bin is assumed to represent
153 snow that is the least affected by LAP and corresponds, thus, most closely to pristine conditions. The fitting was
154 done to $\log(SSA)$ using bins with suitable data coverage (and/or snow cover), therefore excluding low and high
155 temperature bins from the fits (see Figure S2). Calculations were made for both T_s and T_a , but the results proved
156 to be very similar. For simplicity, further correlations are here presented mostly as function of T_a . The
157 dependence of $\log(SSA)$ of air temperature can be written as

$$158 \log(SSA) = -5.92 \cdot 10^{-3} T_a - 0.193 T_a + 1.97 \quad (3)$$

159 where SSA is given in $\text{cm}^2 \text{ g}^{-1}$ and T_a in $^\circ\text{C}$ (the relation $\log(SSA)$ and T_s is provided in the supplement). For a
160 given daily average temperature, equation 3 provides the estimated SSA of the brightest snow surface albedo
161 based on two seasons of data. Those events are thought to occur for relatively young snow without significant
162 influence from LAP. However, this empirical relation will provide the same albedo for young snow at a given
163 daily temperature as for snow that fell at an earlier instance, but with a different temperature for a particular
164 day. After the snow fell, the temperature either increased or decreased. Because eq. 3 only depends on the
165 average temperature of the day, this memory effect is not captured by the parameterization (see additional
166 reasoning in supplement).



167 Through a combination of equations 3, 2, and 1, a projected value of the albedo of near pristine snow and
168 effective grain size, can be derived as function of the air temperature. As T_a increases r_e increases, while a_p
169 decreases.

170

171 3.2 Albedo reduction by LAP

172 With a value for a_p , the subsequent step is to introduce the albedo reduction due to LAP. The empirical relation
173 proposed by Pedersen et al. (2015) is used for the scaling factor of pristine snow

$$174 y_\lambda = A - B x^C \quad (4)$$

175 Where A, B and C are wavelength dependent constants (provided in the supplement section 4). The variable x
176 is

$$177 x = \sqrt{\overline{EC_{eq}} r_e} \quad (5)$$

178 where $\overline{EC_{eq}}$ is the average equivalent EC content (EC plus other LAP) in (ng g^{-1}) in the surface snow and r_e is
179 given in (μm). This parameterization is designed for EC_{eq} concentrations between 1 and 400 ng g^{-1} , but Svensson
180 et al. (2016) has shown that it can be used with reasonable result at significantly higher concentrations.

181 As stated above, in this study the EC_{eq} content includes the albedo reduction from both EC and the equivalent
182 content from other absorbers such as MD, BrC or other light absorbing organic carbon. The concentration or
183 mixing ratios of these species are not known as a function of time a priori. For our measurement site at
184 Sunderdhunga, Svensson et al. (2021) presented evidence of a rather constant mixing ratio of 50 ng g^{-1} of EC in
185 fresh snow and a contribution to light absorption by MD of about 50 %. Thus, we assume that EC_{eq} is equivalent to
186 two times EC. This estimate of $EC_{eq} = 100 \text{ ng g}^{-1}$ is used as our base case throughout this study. An additional
187 assumption is that while snow sublimates and melts, LAP preferentially stays near the surface, as previously
188 observed (e.g. Doherty et al., 2013; Svensson et al., 2016; Xu et al., 2012) in some characteristic depth d (mm)
189 expressed in terms of SWE. The representative or average $\overline{EC_{eq}}$ is then related to the variation in SD according
190 to

$$191 \overline{EC_{eq_n}} = \left(EC_{eq} d + \sum_{i=1}^n SD_i^- \frac{\rho_{ns}}{\rho_w} EC_{eq} \right) / d \quad (6)$$

192 Where SD^- is the absolute change in SD (mm) when i increases, i is the number of day during the snow season
193 and n is the number of days since the start of the snow layer, ρ_{ns} and ρ_w are the density of new snow (100 kg m^{-3})
194 (Helfricht, et al., 2018) and liquid water (1000 kg m^{-3}), respectively. Average EC_{eq} is thus the sum of EC_{eq} in
195 the layer d plus the EC_{eq} that is in layer d from the ablated snow. Therefore, average EC_{eq} depends strongly on
196 the choice of d . A representative d value of 4 mm was determined as explained below in section 3.3. With a
197 value of d , $\overline{EC_{eq}}$ was estimated from the cumulative reduction in SD using eq. 6. When the change in SD is
198 positive (i.e. SD^+) then $\overline{EC_{eq}} = EC_{eq}$. Days with no change in SD were very rare. When this did occur, however,
199 the previous day EC concentration was used. Using $\overline{EC_{eq}}$ from equation 6 when SD is decreasing (SD^-), or the
200 base case when SD is increasing, together with r_e from equation 1, gives x in equation 5. The spectrally



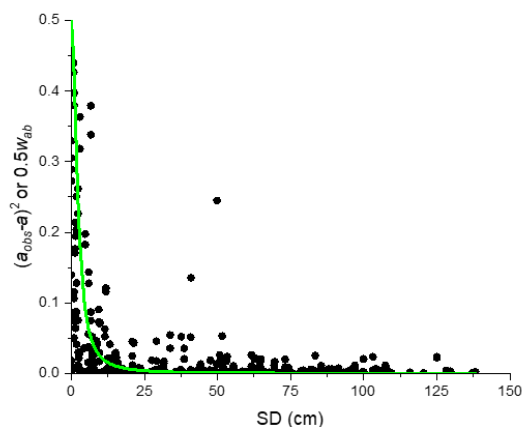
201 dependent y_λ , from equation 4, was weighted over the solar spectrum between 400 and 900 nm using Table 1 of
202 Hulstrom et al. (1985) in order to get the broad band scaling factor y_b . The albedo of the snow containing LAP
203 was then estimated by scaling a_p from eq. 2 with y_b , as

$$204 \quad a = a_p y_b \quad (7)$$

205

206 3.3 Influence from ground albedo and adjustment of parameter d

207 The resulting albedo will depend on the choice of the parameter d , making it imperative to assign a d value that
208 makes the overall difference between observed and estimated albedo a minimum. The observed albedo a_{obs}
209 is compared to a for each day, and the sum of $(a_{obs}-a)^2$ was calculated over the two seasons. By testing different
210 values for d , we aimed to find a value of d that minimizes this sum. The possible influence from the albedo of
211 the ground (a_g) below the snow surface was also considered. In Figure 2, $(a_{obs}-a)^2$ is plotted as a function of SD,
212 where a is calculated with $d=4$ mm. Two sets of data are included using either T_a or T_s to parameterize SSA and
213 r_e (equations S2 and S3). At about SD=50 cm and less, there is some deviation in increased $(a_{obs}-a)^2$, whereas at
214 SD <20 cm it becomes much more apparent. For this reason, SD>55cm data was selected to be used in
215 determining the best value for parameter d .
216



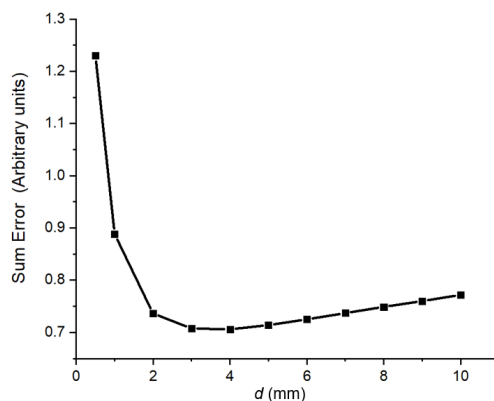
217

218 Figure 2. Presents the squared differences (dots) between observed albedo and the estimated albedo using SD
219 changes and the air temperature or surface temperature as variables. For these calculations a d value of 4 mm
220 was used. The green line is the weighting factor divided by 2, see text for details.

221 Figure 3 presents the variation in the sum of $(a_{obs}-a)^2$ for both seasons using both the T_a and T_s SSA fits, when
222 SD>55 cm. The sums of errors are added for both seasons and both temperature parameterizations. As d
223 increases, the sum decreases down to $d=4$ mm and then slowly increases again for larger d . Hence, a d value of
224 4 mm was selected. This parameter can be viewed as a numerical fix to other shortcomings in the assumptions
225 above, but a physical interpretation of d is that it represents some e-folding thickness of the surface layer where




226 LAP accumulates and interacts with radiation. Since this is expressed as mm SWE, the geometric thickness will
227 depend on snow density. In its physical sense d is not a constant, but depends on the optical properties of the
228 surface snow as well. For instance, a more transparent snow will allow the light to penetrate deeper for the same
229 amount of SWE. This dependence is included to some extent through equation 5, where it is shown that the
230 influence from LAP is enhanced with increasing grain size.



231

232 Figure 3. Sum of errors as function of the parameter d . Errors, $(a_{obs}-a)^2$, are added together for both seasons
233 and both temperature parameterizations of equation S2 and S3. Only data where $SD > 55$ cm are included.

234 To accommodate the obvious influence from the ground albedo (a_g) for small SD , a simple mixing rule was
235 introduced. The snow free a_g is taken as 0.17 (albedo of bare ground before and after snow seasons) which is
236 weighted with a using a factor $w_{a_g} = f(SD)$. This function gives a weight of one at $SD=0$ cm and decreases
237 towards zero as SD increases. The functional dependence of $f(SD)$ is $1 / (1 + \frac{SD^2}{5})$ and presented in Figure 2.
238 As will be evident below (c.f Figure 4), the influence from a_g to albedo is only important at the very start and
239 towards the end of the seasons. This weighting function helps in interpreting the results at either  the
240 seasons, but will not be of great importance for the remainder of the analysis. Therefore, no particular effort to
241 adjust or motivate its shape will be performed. Nevertheless, the final estimated albedo is;

$$242 \quad \text{albedo} = a \left(1 - w_{a_g} \right) + a_g w_{a_g} \quad (8)$$

243

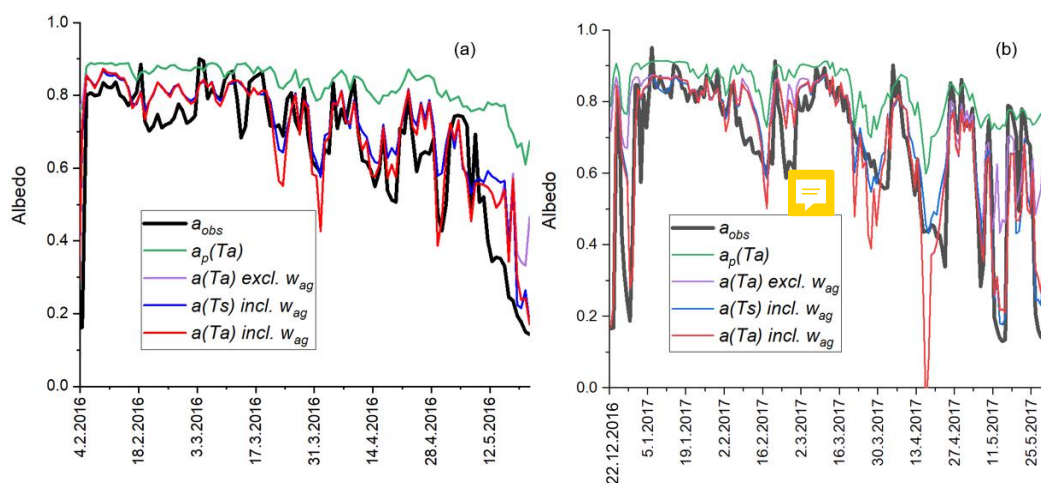
244 3.4 Comparison between observed and parameterized albedo

245 The observed albedo is compared to different parameterized albedos for the two seasons in Figure 4a-b. As
246 expected, the pristine albedo (a_p), indicated by green line, is generally higher than the observed albedo (black
247 line). The pristine albedo does, however, capture the seasonal albedo progression with increase and decrease
248 events fairly well. Shown in Figure 4 is the pristine albedo based on T_a , only because the one derived from T_s is
249 essentially identical. Once the LAP are taken into account using the base case of $EC_{eq}=100$ ng g^{-1} and $d=4$ mm,
250 presented in red and blue lines (red utilizes T_a , while blue T_s in the albedo calculations), the observed albedo is
251 closer matched. In both of these estimates the ground albedo is taken into account. For comparison, a purple



252 line is also displayed to illustrate where the ground albedo (w_{ag} factor) is not taken into account for the albedo
253 calculation. Thus, during periods where the purple line deviates from the red line the ground mainly influences
254 the snow albedo, observed in the beginning and at the end of the study periods.

255 In summary, our results indicate that much of the observed variability in the snow albedo can be reproduced by
256 using only two parameters, T_a and SD. The Pearson correlation coefficient between the observed albedo and
257 $a(T_a)$ including w_{ag} for the two seasons put together is $r^2=0.71$, while when $a(T_s)$ is used $r^2=0.77$ (see Fig. S3).
258



259

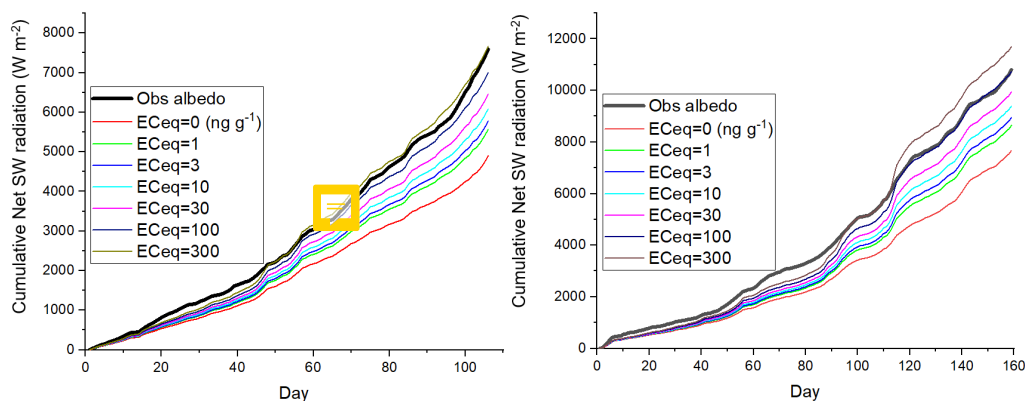
260 Figure 4. The observed albedo and emulated albedo using T_a or T_s with and without LAP and the influence
261 from the underlying surface. Season 1 is presented in panel a), and season 2 is presented in panel b).

262

263 4. Radiative forcing by LAP through the reduction of snow albedo

264 4.1 Relative contribution to net SW radiation due to LAP

265 In this section the cumulative net SW radiation based on the observed incoming and reflected radiation is
266 compared to parameterized cases using different EC_{eq} concentrations. The results are presented in Figure 5a and
267 5b for season 1 and season 2, respectively. It is evident that some of the difference between the observed net
268 SW fluxes and the calculated net SW fluxes estimated based on different EC_{eq} concentrations is manifested
269 already in the beginning of the seasons. This is a period when the sensitivity of net SW radiation to changes in
270 LAP is small. This difference is interpreted as mainly a shortcoming in our simple diagnostic relation eq. 3 to
271 capture the metamorphism of the snow. Because the incoming radiation is low at the start of the seasons, the
272 cumulative effect on the available SW is less than during to the rest of the period. Nonetheless, the seasonal
273 progression is displayed in each season, with the accumulation of LAP throughout the seasons and the
274 subsequent increase in the calculated net SW fluxes. At the end of each season, our base case scenarios are
275 broadly in line with the observed net SW fluxes.

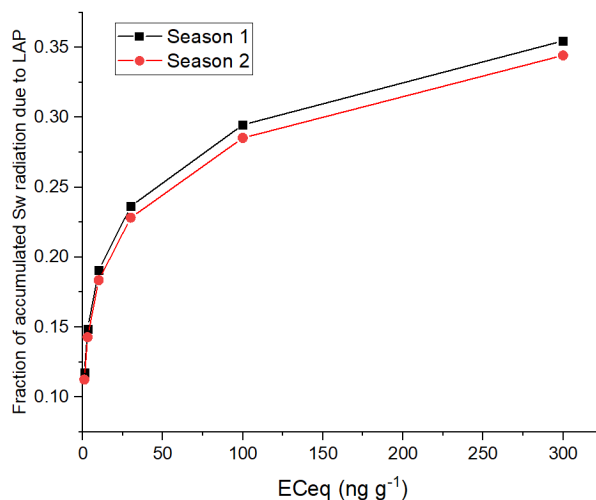


276

277 Figure 5. Cumulative net short wave radiation as a function of daily averaged SW_d calculated based on observed
278 albedo (Obs albedo), and albedo from parameterizations using different values of EC_{eq} . Season 1 and season 2
279 are presented in panels a) and b), respectively.

280 Based on the endpoints in Figure 5a and 5b, the relative contribution from LAP to net SW radiation at the end
281 of the season was calculated as function of EC_{eq} . The results are presented in Figure 6. As EC_{eq} increases, the
282 relative contribution increases. Our base case of EC_{eq} concentration (100 $ng\ g^{-1}$) corresponds to slightly below
283 30% of extra energy accumulated over the entire season for both 1 and 2.

284



285

286 Figure 6. Fractional contribution to net SW radiation reaching the snow as function of EC_{eq} values. Data consists
287 of the end points given in Figure 5.

288 4.2 Melt days

289 All of the extra energy accumulated over the season due to LAP is not available to melt the snow, as a large
290 portion of the incoming energy is returned to the atmosphere as long wave radiation and latent heat.
291 Conceptually, the snow pack increases its black body temperature to compensate for the incoming energy and




292 this temperature increase will to some extent also increase the latent heat flux due to a larger vapor pressure
293 gradient, and at the same time reduce the sensible heat flux due to decreasing temperature gradient. However,
294 this temperature compensation can only continue until some critical temperature is reached and after that the
295 excess energy is used to melt snow. Obviously, 0 °C would constitute such melt threshold and a common method
296 to estimate melt is through the positive degree-day (PDD) concept (e.g. Braithwaite, 1995). The PDD models
297 are formulated in their simplest form as,

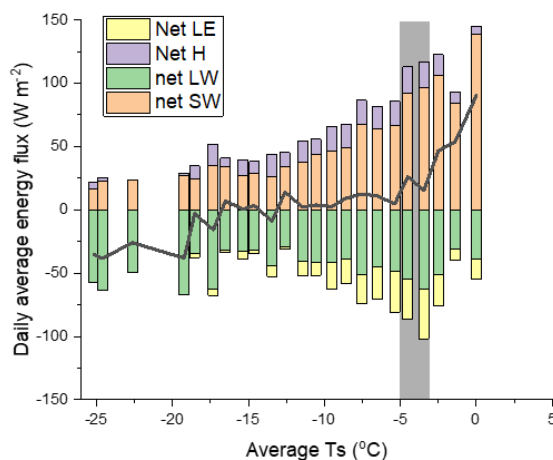


$$M = DDF PDD \quad (9)$$

298 where PDD is the sum of daily mean air temperatures above the melting point, and M is the melt (mm, SWE)
299 over the period of interest, and DDF is the degree-day factor ($\text{mm d}^{-1} \text{ } ^\circ\text{C}^{-1}$).

301 With knowledge on the seasonal M, we can compare the scaling factor, DDF, for our two seasons. This is
302 determined by subtracting the loss of snow due to sublimation from PP, which is done by integrating the latent
303 heat flux (LE) over the season and converting this energy into corresponding amount of SWE using the heat of
304 sublimation (2.848 kJ kg^{-1}). The estimation of latent  flux is presented in the supplement. For season 1 and
305 season 2 the integrated LE losses are equivalent to 46 and 69 mm, respectively. The uncertainties in these values
306 are high due to the simplified estimates of turbulent fluxes. However, they compare well to another study by
307 Stigter et al. (2018), and constitute on average 0.43 and 0.42 mm d^{-1} loss of water to the atmosphere over the
308 time for the seasonal snow cover. Using these estimates of LE, the derived DDF's are 10 ($\text{mm d}^{-1} \text{ } ^\circ\text{C}^{-1}$) for
309 season 1, and 11 ($\text{mm d}^{-1} \text{ } ^\circ\text{C}^{-1}$) for season 2. Compared to other reported values for snow these estimates are
310 high, but are close to those reported for ice (c.f. table 1 of Zhang et al., 2006). A summary of pertinent variables
311 is summarized in Table 1. The number of days with snowmelt using this PDD concept is simply the number of
312 days with an average air temperature above zero. For season 1 this is 14 days and for season 2 this is 26 days.
313 Although the PDD concept indicates a consistency between the two seasons, it provides no direct linkage
314 between the changes in LAP forcing and the air temperature.

315 On the other hand, T_s can be viewed as the response to changes in the energy fluxes. For this, we will explore
316 how the net energy flux changes as function of the black body temperature, T_s to resolve at what threshold
317 temperature the surplus energy is no longer compensated for and is instead available to melt the snow? To
318 investigate this threshold, we combined the observed radiation fluxes and calculated turbulent latent and sensible
319 heat fluxes into their daily net energy fluxes. These four fluxes are presented in Figure 7 as averages over one
320 degree T_s bins. Temperatures above zero are grouped in the 0 °C bin. Warm precipitation, cold content, and
321 geothermic flux are not considered, since all of those are expected to be comparably insignificant at our study
322 case. Similar to the latent heat flux, an estimate of sensible heat flux is presented in supplement section 6.



323

324 Figure 7. The major average energy fluxes for the combined data of Season 1 and Season 2. The black line is
 325 the average net flux for each temperature bin. The gray area marks the temperature range -5 to -3 °C.

326 The average net total energy flux for each degree interval of the black body temperature is overlaid the individual
 327 fluxes in Figure 7. It is worth noting that the absolute value of this total net flux is uncertain, but our interest is
 328 in its variation as a function of T_s . At very cold temperatures below -19 °C (few data points c.f. Fig. S2) there is
 329 a large deficit in the net budget, while at less cold temperatures up to about -5 °C the energy budget is nearly
 330 balanced. In the range -5 to -3 °C there is a shift in the tendency and the net energy surplus increases more
 331 rapidly. This shift in net energy as function of T_s we interpret as the conditions when the snowpack no longer
 332 fully compensates for the additional available energy and the snow starts melting. Days when T_s is greater than
 333 this threshold is defined as days when snowmelt occurs. A temperature of -4 °C will be used as our threshold
 334 value and -5 and -3 °C as our range of uncertainty.

335 Counting the days with $T_s > -4$ (-5, -3) °C, gives 27 (37,19) and 45 (56, 32) days for the respective seasons. This
 336 is about twice the number of days compared with using $T_a > 0$ °C as criteria. The number of days with snowmelt
 337 (#SM) depend on the total amount of precipitation (PP), less the amount of water that is lost from net latent heat
 338 transport to the atmosphere (S). Noteworthy from Table 1, is that the fractions of estimated net S of PP are 0.16
 339 and 0.15 for season 1 and season 2, respectively. Based on the comparable small fractions and the similarity
 340 between seasons, we assume that number of melt days can directly be compared to PP rather than (PP-S) if S
 341 can be described as a single factor multiplied by PP. Dividing our #SM estimates in Table 1 by the PP yields a
 342 #SM per mm PP. The resulting numbers for the two seasons are 0.093 and 0.098 d mm⁻¹ using $T_s > -4$ °C.

343

344 Table 1

Day	PP (mm)	Net Sublimation S (mm)	Fraction S/PP	#SM ^{±Δ#SM} $T_s > -4_{(-4,-3)}^{(-5,-4)} °C$	#SM/PP	Enhanced melt rate by LAP (mm d ⁻¹)
-----	---------	---------------------------	---------------	---	--------	--

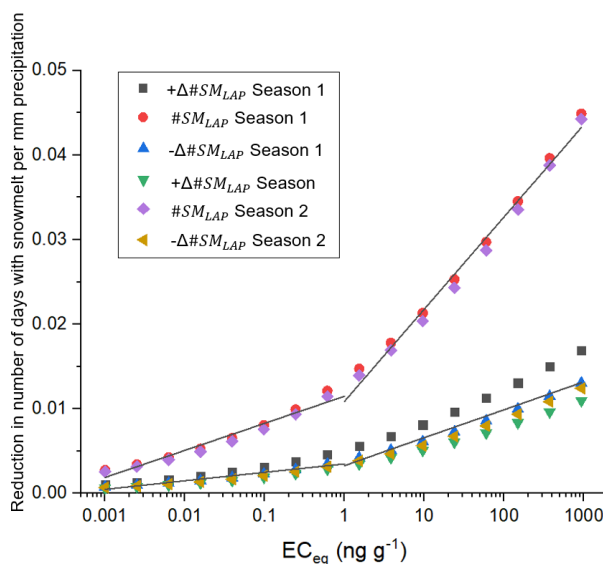


Season 1	106	290	47	0.16	27^{10}_8	$0.093^{0.034}_{0.028}$	2.89
Season 2	159	460	69	0.15	45^{11}_{13}	$0.098^{0.024}_{0.028}$	2.18

345

346 The final step is to estimate the reduction in #SM due to LAP. This was achieved by comparing the accumulated
 347 amount of SW energy over the melt days only, using a range of EC_{eq} values. This is analogous to the presentation
 348 in Figure 6, but taking into account only those days when T_s is above threshold temperature. The respective
 349 LAP contributions are scaled by the #SM/PP factors in Table 1, yielding the estimated contribution to #SM
 350 ($\#SM_{LAP}$) as function of characteristic EC_{eq} in young snow and the seasonal precipitation. These data are
 351 presented in Figure 8 as the reduction in number of days with snowmelt per mm^{-1} as function of EC_{eq} .

352



353

354 Figure 8. The reduction in number of days with snowmelt per mm seasonal precipitation as function of EC_{eq}
 355 concentration in young snow. The straight lines represent the relations in equations 10 through 13, see text for
 356 details.

357 The upper and lower range in $\#SM_{LAP}$ for each season, based on T_s , are presented as $\pm\Delta\#SM_{LAP}$. The
 358 dependence of the contribution to #SM on (EC_{eq}) is non-linear, but dividing the concentration above and below
 359 about 1 ng g^{-1} , reasonable agreement can still be achieved using linear fits and $\log(EC_{eq})$. The four equations
 360 multiplied with PP then become:

361 For $EC_{eq} > 1\text{ ng g}^{-1}$

362
$$\#SM_{LAP} = 0.0109(\log(EC_{eq}) + 1)PP \quad (10)$$

363
$$\pm\Delta\#SM_{LAP} = 0.0033(\log(EC_{eq}) + 1)PP \quad (11)$$

364 For $EC_{eq} \leq 1\text{ ng g}^{-1}$

365
$$\#SM_{LAP} = (0.0032\log(EC_{eq}) + 0.0115)PP \quad (12)$$



$$\pm\Delta\#SM_{LAP} = (0.001\log(EC_{eq}) + 0.0035)PP \quad (13)$$

367

368 Assuming a constant melt rate of the melting period the #SM can be expressed as melt rate. Without the
369 influence of LAP, season 1 would have 27 plus 14 (from eq. 10) days with melting, which yields to total of
370 $(290-47)/(27+14)=6.11$ mm of snowmelt per day. Taking into account the influence of LAP we obtain $(290-$
371 $47)/27=9$ mm per day. This means 2.89 mm extra melt due to LAP. Analogous to this, for season 2 we get 2.18
372 mm per day in extra melt due to LAP.

373

374 5. Discussion and conclusions

375 Based on AWS data and an important assumption of a constant LAP deposition, a set of very simplified
376 equations (10-13) to calculate the shift in snow melt-out date were derived. To arrive at these equations, a first
377 step consisted of displaying that the observed daily variation in albedo could be emulated based on the
378 assumption about constant LAP deposition and only two other variables from the AWS, namely air temperature
379 and snow depth. The follow-up step involved the analysis of the energy balance and temperature response of
380 the snow layer in order to define the period of days with melting snow. By combining the information from this
381 sequence the potential contribution from LAP to the #SM be estimated based on the LAP content and amount
382 of precipitation. With a numerical example using our base case of $EC_{eq}=100$ ng g⁻¹ and a PP of 400 mm gives
383 an advancement of the melt-out date of 13 days ± 4 days (using equations 10 and 11). Because the inversion of
384 DDF includes the contribution from LAP implicitly, this large shift in the #SM used in the PDD concept led to
385 an overestimation of the melting compared to pristine snow.

386 The response in the #SM from changes in LAP is less for very clean snow compared to snow with higher EC_{eq} ,
387 as is visible in the changed slope that occurs around $EC_{eq}=1$ ng g⁻¹ (Fig. 8). For clean snow conditions the
388 reduction is only about 1 day for every 100 mm of precipitate near the 1 ng g⁻¹ intercept. This result suggests
389 that the enhanced melt of seasonal snow cover due to LAP in very clean regions is not very important. When
390 comparing with the shape of the relation in Figure 6, which indicate a very rapid increase in the fraction of
391 energy for small EC_{eq} , this may seem a little contradictive. A plausible explanation is that much of the reduction
392 in albedo during the melt period is from the metamorphism of the snow itself, masking the contribution from
393 LAP, however. This highlights the important insight that LAP can really enhance melting only during the melt
394 period, as previously reported (e.g. Flanner et al., 2007; Jacobi et al., 2015). Our simplistic approach does not
395 take into account all feedback mechanisms, for instance, that LAP enhance snow grain growth. The effect of
396 LAP may in turn be underestimated. Nevertheless, from Figure 4 and 5 it shows that albedo and energy fluxes
397 are reasonable well emulated.

398 The main objective of this study was to address the #SM to changes in LAP. From equation 10 this can be
399 expressed in very general terms. For each doubling of EC_{eq} the melt period is shortened by $0.0109\log(2)PP$ or
400 about $\frac{1}{3}$ of a day per 100 mm precipitation. For our base case $EC_{eq}=100$ ng g⁻¹ and 400 mm precipitation,
401 changing EC_{eq} by a factor two up or down will change the #SM by about $1\frac{1}{3}$ days forward or backward. Changing




402 the LAP content by a factor of two constitute a rather large change if we consider that about half of the LAP
403 was of natural origin through contribution of MD (for the observation site).

404 In the scenario set up for our study region, a large change in anthropogenic deposition is required to achieve a
405 sizeable change in the #SM due to the large background forcing by MD. However, the contribution by EC alone
406 to snowmelt is not small. A shift in the #SM due to half the base case EC_{eq} (with half of the base case constituting
407 representable EC content in the snow at this site) is still 13 days assuming a $PP=400\text{mm}$. Assuming a constant
408 natural MD contribution, a threefold change in anthropogenic EC would be required to increase EC_{eq} a factor
409 of two. Our numerical estimates of the $\#SM_{LAP}$ are broadly in the same range with those reported previously for
410 the Himalaya (e.g. Ménégoz et al., 2014; Zhang et al., 2018; Zhong et al. 2019). In addition, our method allows
411 to estimate the LAP impact on the #SM in a more general form, given that the amount of precipitation and LAP
412 mean deposition are known.

413 On a broader geographical scale, beyond the Himalaya, our results compare well with studies investigating the
414 reduction in snow cover due to LAP in other areas. In the European Alps, Tuzet et al. (2020), estimated a 10 ± 5
415 and 11 ± 1 day shortening of two separate snow seasons in the French Alps using a combination of extensive in-
416 situ observations and process models. Similarly, in the Italian Alps, Di Mauro et al. (2019), reported on an
417 exceptional year with strong MD deposition with LAP advancing the seasonal snow melt by 38 days out of a
418 total 7 months of typical snow duration. This highlights the importance in assessing the anthropogenic influence
419 on the reduction of snow cover duration to further investigate the relative role between EC and MD. An even
420 stronger impact by MD has been estimated for Rocky Mountain snow, Colorado, US (Skiles et al., 2012). For
421 that site the authors suggested as much as a 51 day advancement of the MOD attributed to MD primarily.



422 Data availability

423 All data are available upon request 

424

425 Author contributions

426 JSv, HH, EA, NBD, and HL participated in the collection of field measurements. JSt and JSv analyzed the data
427 and wrote the paper. ST, RH, VPS, ML, HL, and AH took care of project administration. HH, EA, RH, OM, H-
428 WJ, ML, HL, and AH helped with the interpretation of the data. All authors agreed on the content of the paper.

429

430 Competing interests

431 The authors declare that they have no conflict of interest.

432

433 Acknowledgments

434 This work has been supported by the Academy of Finland project: Absorbing Aerosols and Fate of Indian
435 Glaciers (AAFIG; project number 268004), and the Academy of Finland consortium: “Novel Assessment of
436 Black Carbon in the Eurasian Arctic: From Historical Concentrations and Sources to Future Climate Impacts”
437 (NABCEA project number 296302), and the Academy of Finland Flagship (grant no. 337552). JSt is part of the
438 Bolin Centre for Climate Research, and acknowledges the Swedish Research Council grant 2017-03758. JSv
439 acknowledges support from the two foundations Maj and Tor Nessling and Oskar Huttunen, as well as the
440 invited scientist grant from the UGA.



441 References

- 442 Aoki, T., Hachikubo, A., and Hori, M.: Effects of snow physical parameters on shortwave broadband albedos,
443 *J. Geophys. Res.*, 108, 4616, doi:10.1029/2003JD003506, 2003.
- 444 Armstrong, R. L., Rittger, K., Brodzik, M. J., Racoviteanu, A., Barrett, A. P., Khalsa, S.-J. S., Raup, B., Hill,
445 A. F., Khan, A. L., Wilson, A. M., Kayastha, R. B., Fetterer, F., and Armstrong, B.: Runoff from glacier ice
446 and seasonal snow in High Asia: separating melt water sources in river flow, *Reg. Environ. Chang.*, 19,
447 1249–1261, doi.org/10.1007/s10113-018-1429-0, 2019.
- 448 Bonasoni, P., Laj, P., Marinoni, A., Sprenger, M., Angelini, F., Arduini, J., Bonafè, U., Calzolari, F., Colombo,
449 T., Decesari, S., Di Biagio, C., di Sarra, A. G., Evangelisti, F., Duchi, R., Facchini, MC., Fuzzi, S., Gobbi,
450 G. P., Maione, M., Panday, A., Roccatò, F., Sellegri, K., Venzac, H., Verza, G. P., Villani, P., Vuillermoz,
451 E., and Cristofanelli, P.: Atmospheric Brown Clouds in the Himalayas: first two years of continuous
452 observations at the Nepal Climate Observatory-Pyramid (5079 m), *Atmos. Chem. Phys.*, 10, 7515–7531,
453 doi:10.5194/acp-10-7515-2010, 2010.
- 454 Braithwaite, R., Positive degree-day factors for ablation on the Greenland ice sheet studied by energy-balance
455 modelling, *J. Glacio.*, 41, 153-160, 1995.
- 456 Brock, B.W.; Willis, I.C., Sharp, M.J., Measurement and parameterization of albedo variations at Haut Glacier
457 d'Arolla, Switzerland, *J. Glaciol.*, 46, 675-688, 2000.
- 458 Colbeck, S. C.: Grain clusters in wet snow, *J. Colloid Interface Sci.*, 72(3), 371– 384, doi.org/10.1016/0021-
459 9797(79)90340-0, 1979.
- 460 Cuffey, K. and Paterson, W. S. B.: *The Physics of Glaciers*, Elsevier, Butterworth-Heinemann, Burlington, MA,
461 USA, 2010.
- 462 Di Mauro, B., Garzonio, R., Rossini, M., Filippa, G., Pogliotti, P., Galvagno, M., Morra di Cella, U.,
463 Migliavacca, M., Baccolo, G., Clemenza, M., Delmonte, B., Maggi, V., Dumont, M., Tuzet, F., Lafaysse,
464 M., Morin, S., Cremonese, E., and Colombo, R.: Saharan dust events in the European Alps: role in snowmelt
465 and geochemical characterization, *Cryosphere*, 13, 1147–1165, doi.org/10.5194/tc-13-1147-2019, 2019.
- 466 Doherty, S. J., Grenfell, T. C., Forsström, S., Hegg, D. L., Brandt, R. E., and Warren, S. G.: Observed vertical
467 redistribution of black carbon and other insoluble light-absorbing particles in melting snow, *J. Geophys.*
468 *Res.*, 118, 1–17, doi.org/10.1002/jgrd.50235, 2013.
- 469 Emerson, E. W., Katich, J. M., Schwarz, J. P., McMeeking, G. R., and Farmer, D. K.: Direct Measurements of
470 Dry and Wet Deposition of Black Carbon Over a Grassland, *J. Geophys. Res.-Atmos.*, 123, 12277–212290,
471 doi.org/10.1029/2018JD028954, 2018.
- 472 Flanner, M. G., Zender, C. S., Randerson, J. T., and Rasch, P. J.: Present-day climate forcing and response from
473 black carbon in snow, *J. Geophys. Res.-Atmos.*, 112, D11202, doi.org/10.1029/2006JD008003, 2007.
- 474 Forsström, S., Ström, J., Pedersen, C. A., Isaksson, E., and Gerland, S.: Elemental carbon distribution in
475 Svalbard snow, *J. Geophys. Res.-Atmos.*, 114, D19112, doi.org/10.1029/2008JD011480, 2009.
- 476 Gardner, A. S. and Sharp, M. J.: A review of snow and ice albedo and the development of a new physically
477 based broadband albedo parameterization, *J. Geophys. Res.*, 115, F01009, doi:10.1029/2009JF001444, 2010.
- 478 Gertler, C. G., Puppala, S. P., Panday, A., Stumm, D., and Shea, J.: Black carbon and the Himalayan cryosphere:
479 A review, *Atmos. Environ.*, 125, 404–417, doi.org/10.1016/j.atmosenv.2015.08.078, 2016.
- 480 Helfricht, K., Hartl, L., Koch, R., Marty, C., and Olfes, M.: Obtaining sub-daily new snow density from
481 automated measurements in high mountain regions, *Hydrol. Earth Syst. Sci.*, 22, 2655–2668,
482 doi.org/10.5194/hess-22-2655-2018, 2018.



- 483 Hulstrom, R., Bird, R., Riordan, C., Spectral solar irradiance data sets for selected terrestrial conditions. *Solar*
484 *Cells*, 15, 365–391, 1985.
- 485 Jacobi, H.-W., Lim, S., Ménégos, M., Ginot, P., Laj, P., Bonasoni, P., Stocchi, P., Marinoni, A., and Arnaud,
486 Y.: Black carbon in snow in the upper Himalayan Khumbu Valley, Nepal: observations and modeling of the
487 impact on snow albedo, melting, and radiative forcing, *Cryosphere*, 9, 1685–1699, doi.org/10.5194/tc-9-
488 1685-2015, 2015.
- 489 Ménégos, M., Krinner, G., Balkanski, Y., Boucher, O., Cozic, A., Lim, S., Ginot, P., Laj, P., Gallée, H.,
490 Wagon, P., Marinoni, A., and Jacobi, H. W.: Snow cover sensitivity to black carbon deposition in the
491 Himalayas: from atmospheric and ice core measurements to regional climate simulations, *Atmos. Chem.*
492 *Phys.*, 14, 4237–4249, doi.org/10.5194/acp-14-4237-2014, 2014.
- 493 Mimeau, L., Esteves, M., Zin, I., Jacobi, H.-W., Brun, F., Wagon, P., Koirala, D., and Arnaud, Y.:
494 Quantification of different flow components in a high-altitude glacier catchment (Dudh Koshi,
495 Himalaya): some cryospheric-related issues, *Hydrol. Earth Syst. Sci.*, 23, 3969–3996, doi.org/10.5194/hess-
496 23-3969-2019, 2019.
- 497 Ming, J., Cachier, H., Xiao, C., Qin, D., Kang, S., Hou, S., and Xu, J.: Black carbon record based on a shallow
498 Himalayan ice core and its climatic implications, *Atmos. Chem. Phys.*, 8, 1343–1352, doi:10.5194/acp-8-
499 1343-2008, 2008.
- 500 Pedersen, C. A., Gallet, J.-C., Ström, J., Gerland, S., Hudson, S. R., Forsström, S., Isaksson, E., and T. K.
501 Berntsen, T.K.: In situ observations of black carbon in snow and the corresponding spectral surface albedo
502 reduction, *J. Geophys. Res. Atmos.*, 120, 1476–1489, doi:10.1002/2014JD022407, 2015.
- 503 Petzold, A., Ogren, J. A., Fiebig, M., Laj, P., Li, S.-M., Baltensperger, U., Holzer-Popp, T., Kinne, S.,
504 Pappalardo, G., Sugimoto, N., Wehrli, C., Wiedensohler, A., and Zhang, X.-Y.: Recommendations for
505 reporting "black carbon" measurements, *Atmos. Chem. Phys.*, 13, 8365–8379, doi.org/10.5194/acp-13-
506 8365-2013, 2013.
- 507 Sarangi, C., Qian, Y., Rittger, K., Leung, R., Chand, D., Bormann, K. J., Painter, T. H.: Dust dominates high-
508 altitude snow darkening and melt over high-mountain Asia. *Nat. Clim. Chang.* 10, 1045–1051,
509 doi.org/10.1038/s41558-020-00909-3, 2020.
- 510 Schmale, J., Flanner, M., Kang, S., Sprenger, M., Zhang, Q., Guo, J., Li, Y., Schwikowski, M., Farinotti, D.,
511 Modulation of snow reflectance and snowmelt from Central Asian glaciers by anthropogenic black carbon
512 *Sci. Rep.* 7, 40501; doi: 10.1038/srep40501, 2017.
- 513 Schwarz, J. P., Doherty, S. J., Li, F., Ruggiero, S. T., Tanner, C. E., Perring, A. E., Gao, R. S., and Fahey, D.
514 W.: Assessing Single Particle Soot Photometer and Integrating Sphere/Integrating Sandwich
515 Spectrophotometer measurement techniques for quantifying black carbon concentration in snow, *Atmos.*
516 *Meas. Tech.*, 5, 2581–2592, doi.org/10.5194/amt-5-2581-2012, 2012.
- 517 Skiles, S. M., Painter, T. H., Deems, J., Landry, C. & Bryant, A.: Dust radiative forcing in snow of the Upper
518 Colorado River Basin. Part II: interannual variability in radiative forcing and snowmelt rates. *Water Resour.*
519 *Res.* 48, W07522, 2012.
- 520 Stigter, E. E., Maxime Litt, A., Jakob Steiner, F., Pleun Bonekamp, N. J., Joseph Shea, M., and Immerzeel, W.
521 W.: The importance of snow sublimation on a himalayan glacier. *Front. Earth Sci.* 6:108, doi:
522 10.3389/feart.2018.00108, 2018.
- 523 Svensson J., Virkkula A., Meinander O., Kivekäs N., Hannula H.-R., Järvinen O., Peltoniemi J.I., Gritsevich
524 M., Heikkilä A., Kontu A., Neitola K., Brus D., Dagsson-Waldhauserova P., Anttila K., Vehkamäki M.,
525 Hienola A., de Leeuw G. & Lihavainen H.: Soot-doped natural snow and its albedo — results from field
526 experiments. *Boreal Env. Res.* 21: 481–503, 2016.



- 527 Svensson, J., Ström, J., Kivekäs, N., Dkhar, N. B., Tayal, S., Sharma, V. P., Jutila, A., Backman, J., Virkkula,
528 A., Ruppel, M., Hyvärinen, A., Kontu, A., Hannula, H.-R., Leppäranta, M., Hooda, R. K., Korhola, A., Asmi,
529 E., and Lihavainen, H.: Light-absorption of dust and elemental carbon in snow in the Indian Himalayas and
530 the Finnish Arctic, *Atmos. Meas. Tech.*, 11, 1403–1416, doi.org/10.5194/amt-11-1403-2018, 2018.
- 531 Svensson, J., Ström, J., Honkonen, H., Asmi, E., Dkhar, N. B., Tayal, S., Sharma, V. P., Hooda, R., Leppäranta,
532 M., Jacobi, H.-W., Lihavainen, H., and Hyvärinen, A.: Deposition of light-absorbing particles in glacier
533 snow of the Sunderdhunga Valley, the southern forefront of Central Himalaya, *Atmos. Chem. Phys. Discuss.*,
534 doi.org/10.5194/acp-2020-1059, accepted, 2021.
- 535 Tuzet, F., Dumont, M., Picard, G., Lamare, M., Voisin, D., Nabat, P., Lafaysse, M., Larue, F., Revuelto, J., and
536 Arnaud, L.: Quantification of the radiative impact of light-absorbing particles during two contrasted snow
537 seasons at Col du Lautaret (2058 m a.s.l., French Alps), *Cryosphere*, 14, 4553–4579, doi.org/10.5194/tc-14-
538 4553-2020, 2020.
- 539 Warren, S. and Wiscombe, W.: A model for the spectral albedo of snow II. Snow containing atmospheric
540 aerosols, *J. Atmos. Sci.*, 37, 2734–2745, 1980.
- 541 Winter, J.-G., Short- and long-term variability of snow albedo, *Nord. Hydrol.*, 24, 199-212, 1993.
- 542 Xu, B., Cao, J., Joswiak, D.R., Liu, X., Zhao, H., He, J., Zhang, Y., Shiyin, L., Yongjian, D.: Post-depositional
543 enrichment of black soot in snow-pack and accelerated melting of Tibetan glaciers, *Environ. Res. Lett.*, 7,
544 doi:10.1088/1748-9326/7/1/014022, 2012.
- 545 Zhang, Y., Shiyin, L., Yongjian, D., Observed degree-day factors and their spatial variations on glaciers in
546 western China. *Ann. Glaciol.*, 43, 301-306, 2006.
- 547 Zhang, Y., Kang, S., Sprenger, M., Cong, Z., Gao, T., Li, C., Tao, S., Li, X., Zhong, X., Xu, M., Meng, W.,
548 Neupane, B., Qin, X., and Sillanpää, M.: Black carbon and mineral dust in snow cover on the Tibetan Plateau,
549 *Cryosphere*, 12, 413–431, doi.org/10.5194/tc-12-413-2018, 2018.
- 550 Zhong X, Kang S, Zhang W, Yang J, Li X, Zhang Y, Liu Y, Chen P.: Light-absorbing impurities in snow cover
551 across Northern Xinjiang, China, *J. Glaciol.*, 1-18, doi.org/10.1017/jog.2019.69, 2019.
- 552



553		Symbols and acronyms
554		
555	a	Estimated broad band albedo
556	a_{obs}	Observed broad band albedo
557	a_p	Broad band albedo of pristine snow
558	a_g	Broad band albedo of snow free ground
559	AWS	Automatic weather station
560	BC	Black carbon
561	BrC	Brown carbon
562	d	Characteristic depth of surface snow
563	DDF	Degree-day factor
564	EC_{eq}	Elemental carbon equivalent
565	$\overline{EC_{eq}}$	Effective or average EC_{eq}
566	H	Sensible heat flux
567	LAP	Light-absorbing particles
568	LE	Latent heat flux
569	LWu	Long wave radiation up
570	LWd	Long wave radiation down
571	PDD	Positive degree-day
572	PP	Precipitation
573	RH	Relative humidity
574	rBC	Refractory black carbon
575	Re	Effective radius
576	ρ_i	Density of ice
577	ρ_{ns}	Density of new snow
578	ρ_w	Density of water
579	S	Sublimation
580	SD	Snow depth
581	SD ⁻	Decreasing snow depth
582	SD ⁺	Increasing snow depth
583	#SM	Number of days with snowmelt
584	SSA	Specific surface area
585	SWE	Snow water equivalent
586	SWd	Short wave radiation down
587	SWu	Short wave radiation up
588	T_a	Air temperature



589	T_s	Surface temperature
590	U	Wind speed
591	w_{a_g}	Weighting factor between a and a_g
592	y_λ	Spectral albedo reduction due to LAP
593	y_b	Broad band albedo reduction due to LAP